Article

Photonic topological insulator induced by a dislocation in three dimensions

https://doi.org/10.1038/s41586-022-05129-7

Received: 14 December 2021

Accepted: 20 July 2022

Published online: 28 September 2022

Check for updates

Eran Lustig[1,5], Lukas J. Maczewsky[2,5], Julius Beck[2], Tobias Biesenthal[2], Matthias Heinrich[2], Zhaoju Yang[3], Yonatan Plotnik[1], Alexander Szameit[2] & Mordechai Segev[1,4]✉

The hallmark of topological insulators (TIs) is the scatter-free propagation of waves in topologically protected edge channels[1]. This transport is strictly chiral on the outer edge of the medium and therefore capable of bypassing sharp corners and imperfections, even in the presence of substantial disorder. In photonics, two-dimensional (2D) topological edge states have been demonstrated on several different platforms[2–4] and are emerging as a promising tool for robust lasers[5], quantum devices[6–8] and other applications. More recently, 3D TIs were demonstrated in microwaves[9] and acoustic waves[10–13], where the topological protection in the latter is induced by dislocations. However, at optical frequencies, 3D photonic TIs have so far remained out of experimental reach. Here we demonstrate a photonic TI with protected topological surface states in three dimensions. The topological protection is enabled by a screw dislocation. For this purpose, we use the concept of synthetic dimensions[14–17] in a 2D photonic waveguide array[18] by introducing a further modal dimension to transform the system into a 3D topological system. The lattice dislocation endows the system with edge states propagating along 3D trajectories, with topological protection akin to strong photonic TIs[19,20]. Our work paves the way for utilizing 3D topology in photonic science and technology.

Photonic topological insulators (TIs) are systems that facilitate robust and unidirectional flow of light along the edges of the device[2,3,4]. On the basis of similar principles as electronic TIs[1], these artificial electromagnetic media are engineered to exhibit a topologically non-trivial band structure and constitute a promising platform for applications such as forcing extended ensembles of laser emitters to act as one laser[5] and various applications in quantum optics[6,7]. However, unlike electronic TIs, topological photonics has so far mostly relied on one-dimensional (1D)[21] and 2D geometries—essentially confining them to a small subset of possible topological phases. Because photons only interact weakly with surrounding fields, realizing 3D TIs for photons has remained a formidable challenge.

3D TIs that obey time-reversal symmetry are generally divided into two categories: weak and strong[22]. Strong TIs host 3D edge states on all of their surfaces and are impervious to variations in the shape of the medium or disorder that is small compared with the bandgap energy. By contrast, weak 3D TIs are topologically equivalent to stacked arrangements of 2D TIs. In a similar vein, systems lacking time-reversal symmetry may also support 3D TIs by stacking 2D TIs. In the context of bosonic topological systems, these too are considered 'weak', as they do not exhibit topologically protected surface states[20]. For example, a 3D cubic lattice with a constant magnetic field along one of the lattice axes is a weak TI in 3D in the following way (Fig. 1a). Because each of the 2D layers supports an edge state (Fig. 1b), the 3D composite structure is characterized by several edge states propagating on four surfaces. However, the individual edge states couple to one another, giving rise to a dispersion curve on the surface of the lattice. Consequently, the edge states can form a gap, rendering them vulnerable to disorder similar to weak 3D TIs in electronic systems with time-reversal symmetry[23].

Such structures were recently suggested[24–26] and demonstrated[9] with magneto-electric coupling at microwave frequencies. A notable situation occurs when a screw dislocation is introduced into such a system[19] (Fig. 1c). In contrast to the coupling between the planar topological edge states in the pure lattice of a weak TI, the entirety of all the edge states merges into a single edge channel that winds helically around the outer surface of the 3D system. As a result, the phases between neighbouring edges are strictly fixed, preventing the formation of a bandgap and rendering the transport immune to disorder (Fig. 1d). In other words, the dislocation forces the edge states to propagate in all three dimensions and endows the 3D weak TI with topological protection to its edge states[20,27]. Recently, such dislocations in three dimensions were demonstrated in acoustic[10,11], mechanical[12] and electronic systems[13,28], in which 1D topologically protected channels formed between two dislocations in a 3D system.

In photonics, in which magnetic interactions are prohibitively weak at optical frequencies, unorthodox approaches are required to tackle the problem of implementing the physics of TIs on electromagnetic waves[3,4]. Recently, the concept of synthetic dimensions has gained popularity for exploring effects that are otherwise unapproachable owing to limitations in geometry, connectivity and fields in real

[1]Physics Department and Solid State Institute, Technion – Israel Institute of Technology, Haifa, Israel. [2]Institut für Physik, Universität Rostock, Rostock, Germany. [3]Department of Physics, Zhejiang University, Hangzhou, China. [4]Department of Electrical and Computer Engineering, Technion - Israel Institute of Technology, Haifa, Israel. [5]These authors contributed equally: Eran Lustig, Lukas J. Maczewsky. ✉e-mail: msegev@technion.ac.il

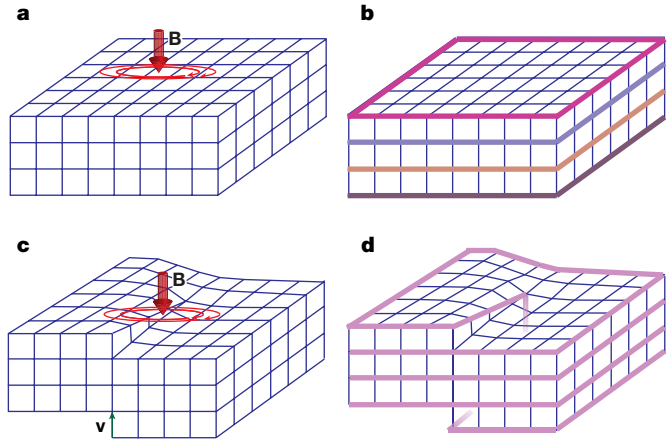

Fig. 1 | A weak TI versus a 3D TI with a dislocation in bosonic systems. a, Illustration of a cubic lattice with a constant magnetic field along one of its axes, which maps to stacking layers of 2D TIs. **b**, Edge states from the different square TIs that can couple to each other and form a gap. **c**, A weak TI (from **a**) with a dislocation defined by the Burgers vector **v**. **d**, In the presence of a screw dislocation, all individual edge states in a weak TI merge into edge states that wind around the entire 3D system. These edge states no longer map to degenerate edge states of a weak TI, but instead give rise to a topologically protected 3D TI.

space[14,29,30]. In photonics, effects requiring three or more dimensions, such as Thouless pumping in high dimensions, Weyl points, disorder in high dimensions and other effects, were successfully demonstrated by reinterpreting certain parameters of the system's Hamiltonian as spatial coordinates[29,31–33]. Alternatively, the use of coupled modal ladders was shown to allow exploring the full dynamics in synthetic space[34,35]. Using this modal ladder technique, photonic TIs[15–17] were demonstrated in hybrid lattices with one spatial axis and one modal axis[18,36]. So far, however, experimental realizations of 3D TIs at optical frequencies remain elusive and, more generally, topologically protected edge states propagating in three dimensions have never been observed with electromagnetic waves.

Here we demonstrate a photonic TI in three dimensions that support topologically protected edge states propagating in 3D trajectories, by virtue of a dislocation. This is also the first realization of a Floquet 3D TI. Hence this work paves the way for both the study of high-dimensional structures in photonics and the interplay of dislocations with topology in general lattice systems. To implement the TI with a dislocation in 3D, we use waveguide lattices with two spatial (x, y) and one modal dimensions. In this configuration, the third spatial coordinate, z, plays the role of time. The evolution of the light is governed by the paraxial wave equation:

$$i\partial_z\psi(x,y,z) = -1/(2k_0)\nabla^2\psi(x,y,z) - (k_0\,\Delta n(x,y,z)\psi(x,y,z))/n_0 \quad (1)$$

in which ψ is the field, k_0 is the wave number in vacuum, n_0 is the ambient refractive index and Δn is the local variation in refractive index that forms the waveguides in our system. To explain how our waveguide structure implements a TI with a dislocation in 3D, we will first describe a single 2D layer lacking dislocations. An individual 2D layer consists of waveguides in a square lattice with lattice constant a (Fig. 2a). Each unit cell in this square lattice includes two waveguides, which rotate around their mean transverse coordinates with a spatial frequency Ω along the propagation axis z, but with a relative phase of π/2. The lattice therefore consists of two sublattices of helical waveguides with a relative phase difference of π/2. Such a structure was shown to be a 2D anomalous Floquet TI[37–39].

To introduce the desired extra dimension, we replace each waveguide in Fig. 2a with a column of waveguides, differing only in their respective effective index of refraction (Fig. 2b,c). This manifests a Stark ladder of modes (Fig. 2d) that, in the following, will serve as the synthetic dimension. The overall structure in real space is shown in Fig. 2e. Crucially, although any column interacts with its neighbouring columns, each mode of each column couples only to a mode

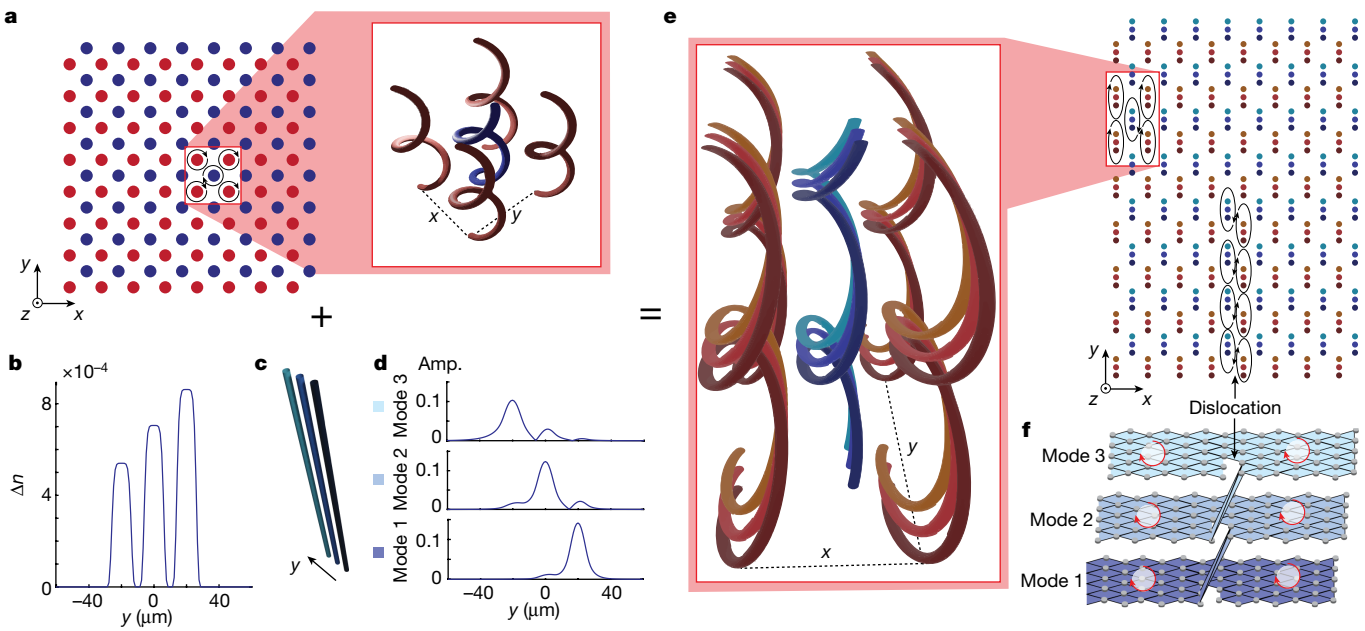

Fig. 2 | Weak TI with photonic waveguide arrays. a, The anomalous quantum Hall effect in a waveguide array as experimentally demonstrated in refs. [38,39]. Each unit cell has two helical waveguides rotating with a phase difference of π/2 between them. **b**,**c**, Gradually increasing refractive index contrast in each column of three waveguides as a function of position along the column, as indicated by the graded blue colours. **d**, Amplitude of the localized modes induced by the index gradient in **b**. **e**, Lattice constructed by replacing each waveguide from **a** with a three-waveguide column from **b**,**c**. The black ellipses represent the location of the centre of the columns in the modulation trajectory, highlighting that the trajectory is shifted by the dislocation. **f**, Synthetic-space diagram of the lattice in **e**, highlighting its correspondence to a 3D weak TI. The synthetic-space lattice contains layers of 2D TIs for each mode. The marked dislocation converts the 3D weak TI to a 3D TI with a dislocation.

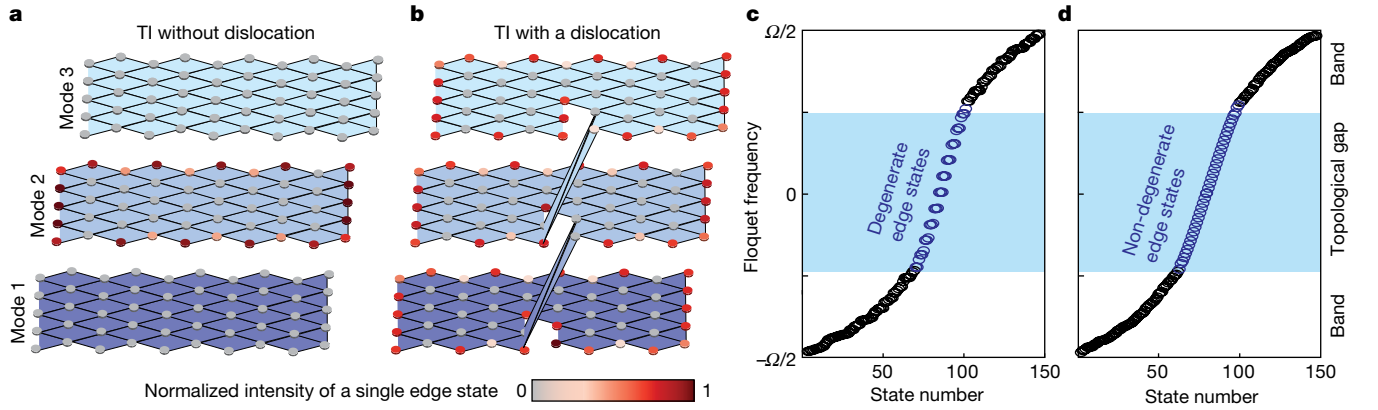

Fig. 3 | 3D TI with a dislocation. a, Formation of an edge state of the three-mode synthetic-space lattice from Fig. 2e without the dislocation (using the experimental parameters in a 5 × 10 lattice). Each mode has a set of 2D edge states of its own. Because the layers are uncoupled, each edge state belongs to a different layer, highlighting that the structure is a weak 3D TI. **b**, Edge states of the weak 3D TI with a dislocation (the lattice of Fig. 2e), formed by the localized coupling between adjacent modes at a specific position. The edge states are extended over the entire 3D lattice. **c**,**d**, Floquet spatial frequency (k_z) for the weak TI in **a** and for the weak TI with a dislocation in **b**, calculated with our experimental parameters. Note that in **c**, the edge states are degenerate (each edge state is in a different layer), whereas in **d**, there is no degeneracy.

with similar wave number k_z because of phase matching. Thus, in the entire lattice, each mode functions as a 2D layer that is weakly coupled to other modes (other 2D layers) owing to the modulation in z (the modulation is slow compared with the lattice spacing in the transverse plane[18]). Furthermore, the parameters Ω and a are chosen such that the 2D lattice of each mode is in the topological phase and is capable of supporting a topological edge state. Consequently, our structure constitutes a 3D weak TI in synthetic dimensions (Fig. 2f) that, before we introduce the dislocation, maps to stacked layers of 2D TIs. To introduce the dislocation, we introduce intermode coupling along a line stretching from the edge to the middle of the lattice. For the intermode coupling to be as efficient as the intramode coupling, we shift the oscillation path and modulate the refractive index, such that at the region of interaction the appropriate waveguides will be phase matched and in proximity (see Methods).

Unlike ordinary weak 3D TI, the edge states in our structure are topologically protected in all three dimensions. The triad of topological invariants associated with our structure is (0, 0, 1), in which the first two invariants are associated with the spatial dimension and the last with the mode dimension, signifying a non-trivial Rudner number[37]. Because the Burgers vector (of the dislocation) points in the direction of the mode ladder and its length is one hopping in the mode ladder, the dislocation induces the topological protection of the surface states of the 3D TI (see Methods). Accordingly, as shown in Fig. 3a, when our waveguide array is devoid of dislocations, the resulting edge states are degenerate and remain strictly confined to individual layers in synthetic space. This can be viewed in Fig. 3c, in which the emerging edge states form degenerate groups of states. In this case, there is no topological protection from localization and other disorder-induced dispersion effects in the mode direction, and a gap can be formed by inducing various perturbations[23].

Introducing a dislocation into this structure changes the situation profoundly. Figure 3b,d shows how the presence of the dislocation affects the structure of the edge states and their respective eigenenergies: the degeneracy is lifted and the resulting dispersive branch diagonally bridges the gap between the bulk bands. Figure 3b also illustrates the path that an edge-wave packet will take: starting at the top layer and moving in a clockwise orientation, an initial excitation will descend to the layer below it each time it encounters the dislocation. Finally, after the lowest modal layer is reached, the wavepacket ascends along the dislocation axis back to the highest mode, thereby completing a genuine 3D loop. In this case, the edge states are topologically protected and thus will not be impaired by interlayer coupling, which naturally exists in our system as a result of the modulation.

We experimentally realize this phenomenon by fabricating the waveguide structure sketched in Fig. 2e using the femtosecond-laser direct-writing technique. To trace the propagation of the light along its protected 3D trajectory, we launch a 633-nm-wavelength laser beam by using a spatial light modulator[40] on the edge of the structure and observe the intensity distribution after 15 cm of propagation at the output facet. We are aiming to show how the light is propagating in a topologically protected fashion in all three dimensions—the two spatial dimensions and the synthetic modal dimension. The propagation of the edge state in the 2D layers is demonstrated with excitations along three segments of the edge-states propagation marked with different colours (Fig. 4a–c). Figure 4a–c sketches the 3D spatial-modal structure, in which each panel corresponds to a different mode. In this figure, we plot the different excitations, in which a filled circle is an excited site, the polygons indicate a segment of the propagation and the roman numerals next to the filled circles indicate a specific excitation with a corresponding output in Fig. 4d–l. Because the modes are tightly localized, the position in modal space can be chosen by injecting light into one of the three waveguides (coloured circles in Fig. 4d–l). Far away from the dislocation, we indeed observe that the excitations remain mostly in their initial modes as they propagate along the edge and around a corner, as shown in the intensity pictures at the output facet of the waveguide array (Fig. 4d–f). Because the modes are localized, we can directly identify the mode from observing the output intensity in the corresponding figure. For example, in Fig. 4c, we excite a wavepacket on the edge such that it is associated with the third mode, by exciting only the lowest waveguide in four columns along the upper edge (excitation I in blue). Accordingly, in the corresponding output (Fig. 4f), the light at the output couples weakly to other modes (that is, it remains at the lower waveguide—mode 3 of each column) and continues to propagate along the edge, bypassing the corner. The same occurs for modes 1 and 2 in excitations I in pink and orange in Fig. 4a,d and Fig. 4b,e, respectively.

It is instructive to view the propagation in modal space near the intersection of the dislocation and the edge (Fig. 4g–i), at which we excite the light near the dislocation, to observe the evolution in the modal dimension. Unlike the excitation presented in Fig. 4d–f, here the light is injected into a certain mode and descends to the mode below it on passing the dislocation (Fig. 4b,h and Fig. 4c,i). The exception is when the beam is launched in the first mode and has no layer to descend

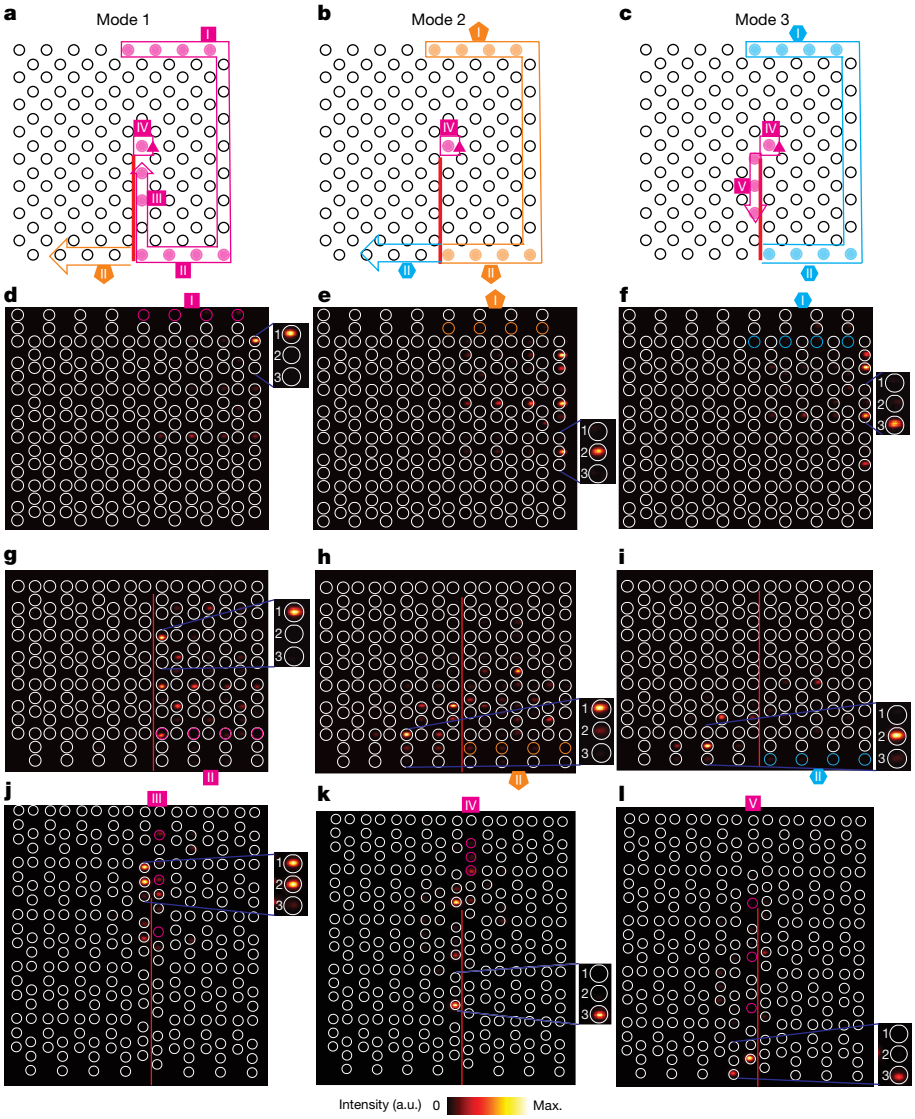

Fig. 4 | Experimentally viewed evolution of edge-wave packets in the 3D synthetic-space TI. a–**c**, Sketches showing the excitation in the synthetic space for modes 1–3, respectively. The filled circles are the excited modes, with each excitation tagged by a different colour and number. The colour marks different segments of the propagations and the numbers mark the chronological order of the excitations. The red line marks the dislocation. **d**–**f**, Intensity images at the output facet of the structure for the excitations numbered I in the three different coloured segments. The coloured circles mark the areas into which light is injected at the input. The light propagates away from the excitation region, passes the corner and continues along the next (vertical) edge. At the output facet, the light is localized in each column in one of the three waveguides, in which the uppermost waveguide of the column represents mode 1 and the lowest waveguide is mode 3. The mode is determined according to the position of the light in the column. **g**–**i**, Same as **d**–**f** but for excitations II in the three coloured segments. Here the excitations lead to the light descending within the modes on the edge near the dislocation. **j**–**l**, Intensity images at the output facet for excitations III, IV and V, respectively, for the pink segment. These excitations show that the light is ascending in the modes along the dislocation and returning to the edge.

to—excitation II in Fig. 4a,g. In this case, the dislocation behaves as a barrier and the light will flow around it (along the dislocation) without scattering, staying in the lowest mode. For example, when launching a wavepacket in mode 2 (light localized on the middle waveguide of each column), near the dislocation, marked by the orange number II in Fig. 4b,h, the light propagates towards the dislocation and then descends to mode 1 (light localized on the upper waveguide of each column) at the other side of it (Fig. 4a), continuing to propagate on the 3D edge. On the other hand, when the light is launched at mode 1 in the same location (excitation II in pink in Fig. 4a,g), the light simply bypasses the dislocation and stays in the same mode—at the upper waveguide.

Finally, we launch a light beam along the dislocation. In this case, instead of descending from mode 3 to mode 1 (as in Fig. 4g–i), the light ascends from mode 1 to mode 3. In Fig. 4a,j, the beam is launched from mode 1 towards the dislocation (excitation III). The output in Fig. 4j shows that the light is occupying mode 2 and localized near the dislocation, as expected. In Fig. 4k (excitation IV), the beam is launched along the dislocation in all modes. In this case, the light ascends to mode 3 and starts to return to encircling the outer circumference of the lattice. Figure 4l (excitation V) shows the rest of the motion, in which the light beam returns from the dislocation and starts to encircle the lattice .

In conclusion, our observations unequivocally show that the topological edge state indeed follows a trajectory in all three dimensions. We experimentally investigated the 3D dynamics of edge states in a photonic TI in 3D and showed that the introduction of a screw dislocation endows the system with topological protection. This is the first observation of a photonic TI in 3D with topologically protected edge

states and also the first photonic TI in 3D synthetic space. We expect that this work will open the door for exploring higher-dimensional topological phases in laboratory experiments.

Online content

Any methods, additional references, Nature Research reporting summaries, source data, extended data, supplementary information, acknowledgements, peer review information; details of author contributions and competing interests; and statements of data and code availability are available at https://doi.org/10.1038/s41586-022-05129-7.

1. König, M. et al. Quantum spin Hall insulator state in HgTe quantum wells. *Science* **318**, 766–770 (2007).
2. Wang, Z., Chong, Y., Joannopoulos, J. D. & Soljačić, M. Observation of unidirectional backscattering-immune topological electromagnetic states. *Nature* **461**, 772–775 (2009).
3. Rechtsman, M. C. et al. Photonic Floquet topological insulators. *Nature* **496**, 196–200 (2013).
4. Hafezi, M., Mittal, S., Fan, J., Migdall, A. & Taylor, J. M. Imaging topological edge states in silicon photonics. *Nat. Photon.* **7**, 1001–1005 (2013).
5. Bandres, M. A. et al. Topological insulator laser: experiments. *Science* **359**, eaar4005 (2018).
6. Barik, S. et al. A topological quantum optics interface. *Science* **359**, 666–668 (2018).
7. Blanco-Redondo, A., Bell, B., Oren, D., Eggleton, B. J. & Segev, M. Topological protection of biphoton states. *Science* **362**, 568–571 (2018).
8. Wang, M. et al. Topologically protected entangled photonic states. *Nanophotonics* **8**, 1327–1335 (2019).
9. Yang, Y. et al. Realization of a three-dimensional photonic topological insulator. *Nature* **565**, 622–626 (2019).
10. Xue, H. et al. Observation of dislocation-induced topological modes in a three-dimensional acoustic topological insulator. *Phys. Rev. Lett.* **127**, 214301 (2021).
11. Ye, L. et al. Topological dislocation modes in three-dimensional acoustic topological insulators. *Nat. Commun.* **13**, 508 (2022).
12. Wang, W., Chen, Z.-G. & Ma, G. Synthetic three-dimensional $Z\times Z_2$ topological insulator in an elastic metacrystal. *Phys. Rev. Lett.* **127**, 214302 (2021).
13. Nayak, A. K. et al. Resolving the topological classification of bismuth with topological defects. *Sci. Adv.* **5**, eaax6996 (2019).
14. Boada, O., Celi, A., Latorre, J. I. & Lewenstein, M. Quantum simulation of an extra dimension. *Phys. Rev. Lett.* **108**, 133001 (2012).
15. Luo, X.-W. et al. Quantum simulation of 2D topological physics in a 1D array of optical cavities. *Nat. Commun.* **6**, 7704 (2015).
16. Ozawa, T., Price, H. M., Goldman, N., Zilberberg, O. & Carusotto, I. Synthetic dimensions in integrated photonics: from optical isolation to four-dimensional quantum Hall physics. *Phys. Rev. A* **93**, 43827 (2016).
17. Yuan, L., Shi, Y. & Fan, S. Photonic gauge potential in a system with a synthetic frequency dimension. *Opt. Lett.* **41**, 741–744 (2016).
18. Lustig, E. et al. Photonic topological insulator in synthetic dimensions. *Nature* **567**, 356–360 (2019).
19. Ran, Y., Zhang, Y. & Vishwanath, A. One-dimensional topologically protected modes in topological insulators with lattice dislocations. *Nat. Phys.* **5**, 298–303 (2009).
20. Lu, L. & Wang, Z. Topological one-way fiber of second Chern number. *Nat. Commun.* **9**, 5384 (2018).
21. Malkova, N., Hromada, I., Wang, X., Bryant, G. & Chen, Z. Observation of optical Shockley-like surface states in photonic superlattices. *Opt. Lett.* **34**, 1633–1635 (2009).
22. Fu, L., Kane, C. L. & Mele, E. J. Topological insulators in three dimensions. *Phys. Rev. Lett.* **98**, 106803 (2007).
23. Ringel, Z., Kraus, Y. E. & Stern, A. Strong side of weak topological insulators. *Phys. Rev. B* **86**, 45102 (2012).
24. Slobozhanyuk, A. et al. Three-dimensional all-dielectric photonic topological insulator. *Nat. Photon.* **11**, 130–136 (2017).
25. Lin, Q., Sun, X.-Q., Xiao, M., Zhang, S.-C. & Fan, S. Constructing three-dimensional photonic topological insulator using two-dimensional ring resonator lattice with a synthetic frequency dimension. *Sci. Adv.* **4**, eaat2774 (2018).
26. Khanikaev, A. B. et al. Photonic topological insulators. *Nat. Mater.* **12**, 233–239 (2012).
27. Teo, J. C. Y. & Kane, C. L. Topological defects and gapless modes in insulators and superconductors. *Phys. Rev. B* **82**, 115120 (2010).
28. Hamasaki, H., Tokumoto, Y. & Edagawa, K. Dislocation conduction in Bi-Sb topological insulators. *Appl. Phys. Lett.* **110**, 92105 (2017).
29. Kraus, Y. E., Lahini, Y., Ringel, Z., Verbin, M. & Zilberberg, O. Topological states and adiabatic pumping in quasicrystals. *Phys. Rev. Lett.* **109**, 106402 (2012).
30. Jukić, D. & Buljan, H. Four-dimensional photonic lattices and discrete tesseract solitons. *Phys. Rev. A* **87**, 13814 (2013).
31. Noh, J. et al. Experimental observation of optical Weyl points and Fermi arc-like surface states. *Nat. Phys.* **13**, 611–617 (2017).
32. Maczewsky, L. J. et al. Synthesizing multi-dimensional excitation dynamics and localization transition in one-dimensional lattices. *Nat. Photon.* **14**, 76–81 (2020).
33. Zilberberg, O. et al. Photonic topological boundary pumping as a probe of 4D quantum Hall physics. *Nature* **553**, 59–62 (2018).
34. Stuhl, B. K., Lu, H.-I., Aycock, L. M., Genkina, D. & Spielman, I. B. Visualizing edge states with an atomic Bose gas in the quantum Hall regime. *Science* **349**, 1514–1518 (2015).
35. Mancini, M. et al. Observation of chiral edge states with neutral fermions in synthetic Hall ribbons. *Science* **349**, 1510–1513 (2015).
36. Dutt, A. et al. A single photonic cavity with two independent physical synthetic dimensions. *Science* **367**, 59–64 (2020).
37. Rudner, M. S., Lindner, N. H., Berg, E. & Levin, M. Anomalous edge states and the bulk-edge correspondence for periodically driven two-dimensional systems. *Phys. Rev. X* **3**, 31005 (2013).
38. Maczewsky, L. J., Zeuner, J. M., Nolte, S. & Szameit, A. Observation of photonic anomalous Floquet topological insulators. *Nat. Commun.* **8**, 13756 (2017).
39. Mukherjee, S. et al. Experimental observation of anomalous topological edge modes in a slowly driven photonic lattice. *Nat. Commun.* **8**, 13918 (2017).
40. Biesenthal, T., Kremer, M., Heinrich, M. & Szameit, A. Experimental realization of PT-symmetric flat bands. *Phys. Rev. Lett.* **123**, 183601 (2019).

Methods

Design

In this section, we explain the process of designing the 3D photonic TI. This design relies on the concept of synthetic dimensions[14,41] on the platform of waveguide arrays[18,42].

Our lattice is periodic (except for the dislocation) with lattice displacement vectors:

$$\mathbf{a} = (a_x, a_y)/2,\ \mathbf{d}_1 = a_x(1, 0),\ \mathbf{d}_2 = a_y(0, 1) \quad (1)$$

in which a_x and a_y are the lattice constants, $\mathbf{d}_1$ and $\mathbf{d}_2$ are the primitive vectors and $\mathbf{a}$ is the displacement vector within the unit cell. Each 'site' in our lattice is a column of three waveguides, equally distant from one another, separated by distance ΔS (Extended Data Fig. 1a). Our lattice is periodically modulated in the propagation direction z such that, in each period, each column exchanges energy with its four neighbouring columns in a clockwise (or counterclockwise) manner, which—in turn—induces anomalous edge states[37–39,43]. The trajectory of the waveguides in space is helical with an 'hourglass' projection on the x–y plane. We control the effective coupling between each column of waveguides and its neighbours by adjusting the 'hourglass' contour in the x–y plane while maintaining the periodicity in the propagation direction. The size of ΔS is dictated by a balance between the need to have both localized modes and confined trajectories to reduce losses.

To obtain the gradient in the refractive index in each column (indicated by the size of the sites in Extended Data Fig. 1a; larger circles represent deeper waveguides), we use different writing speeds, which result in different index contrast for each site (Extended Data Fig. 1b). This translates into different coupling coefficients for different waveguides, hence it is essential to make sure that each mode is in the topological phase, despite the different index contrasts. We do that by tuning the spatial oscillation frequency of the waveguides Ω and the other parameters. We design the system with tight-binding simulations and follow up with paraxial beam-propagation simulations of the entire structure (the tight-binding simulations are presented Fig. 3a–d). Specifically, along the line of the dislocation, the waveguides are shifted at the point of closest proximity (Extended Data Fig. 1c). Near this point, the index is varied gradually and adiabatically in both columns in the unit cell, such that phase-matching conditions are satisfied (see size of the circles in the Extended Data Fig. 1c).

Fabricated structure

We use 15-cm-long samples of fused silica glass (Corning 7980) and fabricate the structure using the femtosecond-laser writing method[44]. We use 140-fs pulses created by a Ti:sapphire Coherent Vitara-S laser and amplified by a Coherent RegA optical parametric amplifier. Each pulse carries energy of 270 nJ at 800 nm, at a 100-kHz repetition rate. The focus of the laser beam generated by a 20× objective (0.35 numerical aperture) is translated in the glass sample using a high-precision positioning stage (Aerotech ALS180/130).

Dimensions of the lattice and waveguides trajectory

The lattice dimensions are given by $a_x = 49.56$ μm and $a_y = 80$ μm and the spatial frequency Ω is 1.163 cm^{-1}. The lattice is composed of 8×8 unit cells, each with six waveguides arranged in two columns. The distance between neighbouring waveguides in each column is $\Delta S = 22$ μm. The helical 'hourglass' trajectory (green dashed line in Extended Data Fig. 1a,c) is constructed with the two vectors $\mathbf{p}_1(\tilde{z})$ and $\mathbf{p}_2(\tilde{z})$, in which $\tilde{z}$ is a unitless z-coordinate that changes from 0 to 1. These functions correspond to the line and curve of the helical 'hourglass' shape, respectively:

$$\mathbf{p}_{1x}(\tilde{z}) = \pm x_p/2 \cdot \mathrm{sign}(\tilde{z}) \cdot |\tilde{z}|^{(0.8-0.3\tilde{z})} \quad (2)$$

$$\mathbf{p}_{1y} = \mp y_p/2 \quad (3)$$

$$\mathbf{p}_{2x}(\tilde{z}) = \pm x_p(1/2 - 0.4 \cdot |\cos(\pi(\mathrm{sign}(\tilde{z}) \cdot |\tilde{z}|)/2)|) \quad (4)$$

$$\mathbf{p}_{2y}(\tilde{z}) = \pm y_p/2(\mathrm{sign}(\tilde{z}) \cdot |\tilde{z}|^{(2/5|\tilde{z}^{1/3})}| + (1 - |\tilde{z}^{1/3}|)) \quad (5)$$

in which equations (2)–(5) present the components of the vectors $\mathbf{p}_1$ and $\mathbf{p}_2$.

In our case, the parameters that dictate the dimensions of the 'hourglass' are $x_p = 9.69$ μm and $y_p = 40$ μm and the exponential terms multiplying $|z|$ control the transverse derivative $\nabla_\perp$. Recalling that z is equivalent to time in the corresponding Schrödinger equation, these terms represent the velocity in the x–y plane. This velocity should both induce proper coupling so that the structure is in the topological phase and, at the same time, it should also be low enough to reduce radiation losses (coupling to unbound waves outside the structure), such that the edge states should still be able to show considerable evolution during their propagation in the finite structure.

Numerical analysis of intermodal coupling

Unlike 3D 'strong TIs'[1,45–49], weak TIs in systems that obey time-reversal symmetry suffer from the possibility that their edge states will gap in the presence of interlayer coupling and disorder. Similarly, when our structure is absent of the dislocation, interlayer coupling or disorder may disrupt the transport of the edge states. However, on introducing the dislocation to the system, robust edge states are formed and show topological protection.

To demonstrate this phenomenon, we numerically analyse the effect of intermodal coupling between different modes of the three-waveguide structure (each individual waveguide has a single guided mode) in the structure used in our experiments on the photonic TI in 3D.

We find that this intermodal coupling is reduced because of the slightly different refractive index contrast defining different waveguides, which results in large phase mismatch between the modes. Specifically, our structure, see Fig. 2b–d, shows that the refractive index contrast defining the three waveguides is around $(5, 7, 9) \times 10^{-4}$ on a substrate of $n = 1.45$, which is manifested in a 'coherence length' (propagation distance after which the phase mismatch is π) of about 1.5 mm. Essentially, had we used straight waveguides (instead of the helical waveguides), the intermodal coupling would have been zero. However, because our waveguides are helical, the intermodal coupling is not zero, in fact, it is not negligible. Because the synthetic modes are of the static lattice, the helicity of the waveguides (acting as modulation along z) introduces coupling between them. Fortunately, the topological design is meant to cope with such coupling and the edge states are robust to it. Thus, although the coupling can introduce some intermodal transport of the light propagating in the 3D structure, the unidirectional flow on the edge is unaffected. In fact, the topological protection only truly works because of the dislocation, which is necessary for the topological protection of the edge states on the surface of the 3D structure in synthetic space[19,27,50,51]. Beyond the topological analysis described in this Methods section, an exact mechanism in which the protection is lost if the dislocation is absent from our system is addressed in Fig. 1 and in the following discussion. As shown in Figs. 1 and 3, without dislocation and without intermodal coupling, the topological surface states that encircle the bulk are composed of 1D degenerate edge states that are attributed to each 2D layer. Thus, although the spectrum of the topological surface states with the dislocation is linearly ascending (Fig. 3d) with the state number, the spectrum without the dislocation exhibits a collection of groups of degenerate edge states (Fig. 3c). Extended Data Figure 2 shows the spectrum and the typical edge-states occupancy on the lattice when introducing interlayer coupling. In Extended Fig. 2a–d, we introduce

moderate interlayer coupling that is 20% of the coupling between lattice sites in both cases of lattices without dislocation (Extended Data Fig. 2a,c) and with dislocation (Extended Data Fig. 2b,d). Extended Data Figure 2e–h shows the spectrum and edge-states occupancy for strong interlayer coupling of 60%. In the absence of dislocation, the resulting topological surface states are completely trivial in the mode dimension, hence the coupling introduces trivial dispersion between the 1D edge states that impairs the surface states.

The consequence in the trivial case is having modes that are not evenly distributed on the entire surface in the synthetic (modal) dimension, which obstruct the propagation on the entire surface. In fact, the structure of the spectrum in the modal space is sensitive and can be altered strongly and unexpectedly by having different interlayer couplings, and is also prone to Anderson localization. These properties are detrimental when using topological edge states for applications such as TI lasers[5,52–55] and topologically protected quantum states[6–8,56,57], which require fixed phase relation, fully extended states and smooth linear dispersion. Furthermore, the protection affects a plethora of 3D-related relevant effects, such as that of non-linearities[58] and localization in 3D (ref. [59]). The situation is even more pronounced when tailored (non-random) perturbations are introduced[23]; these can open the (trivial) gap and cause localization along the edges in the spatial dimension, thereby breaking the protection of the edge states.

The situation is completely different when a dislocation attached to the edge is present in the structure. In this case, there is true topological protection and the topological surface states remain equally spaced in the mode space even for strong interlayer coupling and in the presence of disorder. This happens because the degeneracy of different layers is broken by a dislocation that respects the phase differences required to close a loop. Hence, it is the dislocation that makes the topological surface states ideal, with a smooth linear spectrum that is not prone to localization along the modal dimension in addition to the topological protection in the spatial plane.

Analytic and topological analysis

In this section, we give an analytic description of our experimental photonic TI in three dimensions. We first describe the 2D photonic TI occurring separately for each mode of the column of waveguides. Assuming no dislocation, each mode couples mostly to the same mode in the columns of waveguides that are in its proximity. Thus, for each mode, there is a 2D lattice of waveguides that is a bipartite lattice with 'driving' that is similar, but not the same, as described in refs. [37,38,60]. A driving cycle can be divided into four parts, in which in each part each column interacts by proximity with one of its four neighbouring columns in a clockwise order. Thus, the 2D Hamiltonian for each mode is:

$$H_m^{2D}(k,z) = -\sum_{j=1}^{4}\begin{pmatrix} 0 & c_j^m(z)e^{i\mathbf{b}_j k} \\ c_j^m(z)e^{-i\mathbf{b}_j k} & 0 \end{pmatrix} \quad (6)$$

in which the vectors $\{\mathbf{b}_j\}$ are given by $\mathbf{b}_1 = (a, 0)$, $\mathbf{b}_2 = (0, a)$, $\mathbf{b}_3 = -\mathbf{b}_1$, $\mathbf{b}_4 = -\mathbf{b}_2$, and a is the lattice constant. $c_j^m(z)$ are the coupling coefficients of mode m, which are assumed for simplicity to be non-zero only at a specific $z = \{0, Z/4, Z/2, 3Z/4\}$ in each period, with Z being the period length. Because the Hamiltonian is periodic in z, which plays the role of time, we use the Floquet theorem to find the quasi-momentum values k_z that are analogous to quasi-energy values in a time-dependent system. The evolution in z is given by

$$\psi(z) = P\exp[-i\int_0^z H(\zeta)d\zeta]\psi(0) = U(z)\psi(0) \quad (7)$$

in which ψ is the wavefunction of the light beam and P is a z-ordering operator. The effective Hamiltonian H_{eff} is obtained by the z evolution U over a period given by equation (7). The corresponding effective Hamiltonian describes a 2D TI with chiral edge states characterized by the winding number[37]:

$$W[U] = \frac{1}{8\pi^2}\int dz dk_x dk_y \mathrm{Tr}(U^{-1}\partial_z U[U^{-1}\partial_{k_x}U, U^{-1}\partial_{k_y}U]) \quad (8)$$

We judicially design the parameters $c_j^m(z)$ (see Methods) such that the winding number is 1 for each mode. Furthermore, the edge states predicted by equation (8) appear only in the case that the infinite system described by equation (6) is truncated such that it becomes finite. Next, we construct our 3D Hamiltonian by taking into account the several modes m that exist in our system and describe it in terms of equation (6) as follows:

$$H^{3D} = \sum_m H_m^{2D} + C \quad (9)$$

in which C is the matrix that represents the intermodal coupling that arises from the helical motion of the columns of waveguides, and it depends on the x–y lattice site, mode and z. In the ideal case, when the modes are well separated in k_z and the motion is adiabatic, C can be neglected. H^{3D} manifests stacking of 2D photonic TIs. The entire system is gapped if C is small enough and does not close the bandgap. In this case, the edge states experience trivial dispersion on the surfaces of the 3D space constructed from two spatial dimensions, the location of the column in xy and the mode dimension m. This structure can be described by a triad of topological indices for the three directions:

$$n_1 = W^{ym}(k_x),\ n_2 = W^{xm}(k_y),\ n_3 = W^{xy}(km) \quad (10)$$

in which in our case only n_3 is non-trivial and $n_1 = n_2 = 0$. As mentioned in the previous part of the Methods, the surface state of the structure experiences trivial dispersion that can form a gap and deform (along the mode axis) because of the intermodal coupling C. To make the surface state topologically protected and extended to cover the entire surface of the 3D structure, we introduce a dislocation in the middle of the structure such that the dislocation is connected to the surface state[25,27,50,51]. Taking $\mathbf{B}$ to be the Burgers vector of the dislocation, the 3D TI with indices $\mathbf{n} = (n_1, n_2, n_3)$ has $\mathbf{n}\cdot\mathbf{B}$ topologically protected modes along the dislocation. These protected modes are the same as those on the surface, as the dislocation is connected to the surface. In our system, the Burgers vector of the dislocation is given by $\mathbf{B} = (0, 0, 1)$, because it is stretched along one site in the mode dimension. Thus, our system has $\mathbf{n}\cdot\mathbf{B} = 1$ topological surface state (one dispersion line crossing the bandgap).

Data availability

The data that support the findings of this study are available from the corresponding author upon reasonable request.

41. Celi, A. et al. Synthetic gauge fields in synthetic dimensions. *Phys. Rev. Lett.* **112**, 043001 (2014).
42. Lustig, E. et al. in *Conference on Lasers and Electro-Optics*, paper FW3A.2 (Optical Society of America, 2020).
43. Leykam, D., Rechtsman, M. C. & Chong, Y. D. Anomalous topological phases and unpaired Dirac cones in photonic Floquet topological insulators. *Phys. Rev. Lett.* **117**, 13902 (2016).
44. Szameit, A. et al. Discrete optics in femtosecond-laser-written photonic structures. *J. Phys. B At. Mol. Opt. Phys.* **43**, 163001 (2010).
45. Bernevig, B. A., Hughes, T. L. & Zhang, S.-C. Quantum spin Hall effect and topological phase transition in HgTe quantum wells. *Science* **314**, 1757–1761 (2006).
46. Hasan, M. Z. & Kane, C. L. Colloquium: Topological insulators. *Rev. Mod. Phys.* **82**, 3045–3067 (2010).
47. Moore, J. E. & Balents, L. Topological invariants of time-reversal-invariant band structures. *Phys. Rev. B* **75**, 121306 (2007).
48. Hsieh, D. et al. A topological Dirac insulator in a quantum spin Hall phase. *Nature* **452**, 970–974 (2008).
49. Roy, R. Topological phases and the quantum spin Hall effect in three dimensions. *Phys. Rev. B* **79**, 195322 (2009).

50. Bi, R., Yan, Z., Lu, L. & Wang, Z. Topological defects in Floquet systems: anomalous chiral modes and topological invariant. *Phys. Rev. B* **95**, 161115 (2017).
51. Nag, T. & Roy, B. Anomalous and normal dislocation modes in Floquet topological insulators. *Commun. Phys.* **4**, 157 (2021).
52. Harari, G. et al. in *Conference on Lasers and Electro-Optics*, paper FM3A.3 (Optical Society of America, 2016).
53. Bahari, B. et al. Nonreciprocal lasing in topological cavities of arbitrary geometries. *Science* **358**, 636–640 (2017).
54. Harari, G. et al. Topological insulator laser: theory. *Science* **359**, eaar4003 (2018).
55. Dikopoltsev, A. et al. Topological insulator vertical-cavity laser array. *Science* **373**, 1514–1517 (2021).
56. Mittal, S., Orre, V. V. & Hafezi, M. Topologically robust transport of entangled photons in a 2D photonic system. *Opt. Express* **24**, 15631–15641 (2016).
57. Dai, T. et al. Topologically protected quantum entanglement emitters. *Nat. Photon.* **16**, 248–257 (2022).
58. Christodoulides, D. N. & Joseph, R. I. Discrete self-focusing in nonlinear arrays of coupled waveguides. *Opt. Lett.* **13**, 794–796 (1988).
59. Schwartz, T., Bartal, G., Fishman, S. & Segev, M. Transport and Anderson localization in disordered two-dimensional photonic lattices. *Nature* **446**, 52–55 (2007).
60. Afzal, S. & Van, V. Trapping light in a Floquet topological photonic insulator by Floquet defect mode resonance. *APL Photonics* **6**, 116101 (2021).

Acknowledgements We would like to thank C. Otto for preparing the high-quality fused silica samples used for the inscription of all photonic structures in this work. The Technion team gratefully acknowledges the support of an Advanced Grant from the European Research Council (ERC) under the European Union's Horizon 2020 research and innovation programme (grant agreement no. 789339) and the support of a research grant from the Air Force Office of Scientific Research (AFOSR) of the USA. The Rostock team gratefully acknowledges the support of the Deutsche Forschungsgemeinschaft (grants SCHE 612/6-1, SZ 276/12-1, BL 574/13-1, SZ 276/15-1, SZ 276/20-1 and SFB 1477 'Light-Matter Interactions at Interfaces', project number 441234705) and the Alfried Krupp von Bohlen und Halbach Foundation.

Author contributions Eran Lustig and Lukas J. Maczewsky contributed equally to this work. All authors contributed substantially to this work.

Competing interests The authors declare no competing interests.

Additional information

Correspondence and requests for materials should be addressed to Mordechai Segev.

Peer review information *Nature* thanks Avik Dutt, Alexander Khanikaev and the other, anonymous, reviewer(s) for their contribution to the peer review of this work.

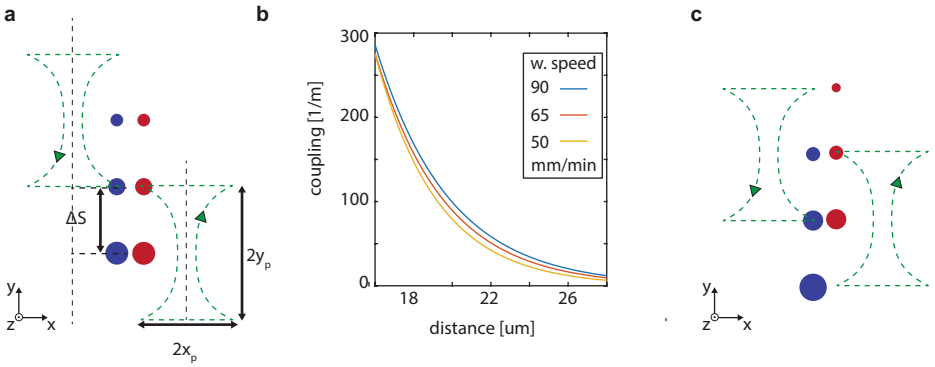

Extended Data Fig. 1 | Unit cell of the 3D photonic TI. a, The dashed green line is the projection of the trajectory of the two columns of waveguides (blue and red) on the *x*–*y* plane. The directions of the helical motion follow the green arrowheads. The two columns are presented here at their closest proximity to one another along the trajectory. The size of each waveguide indicates the different 'depth' of refractive index (the largest circle is the deepest waveguide). **b**, Coupling between adjacent waveguides as a function of their *x* separation, obtained by different speeds of the laser-writing process, which translates into different refractive index contrast. **c**, Same as **a** but at the dislocation, at which the shift creates coupling between localized modes of different 2D layers.

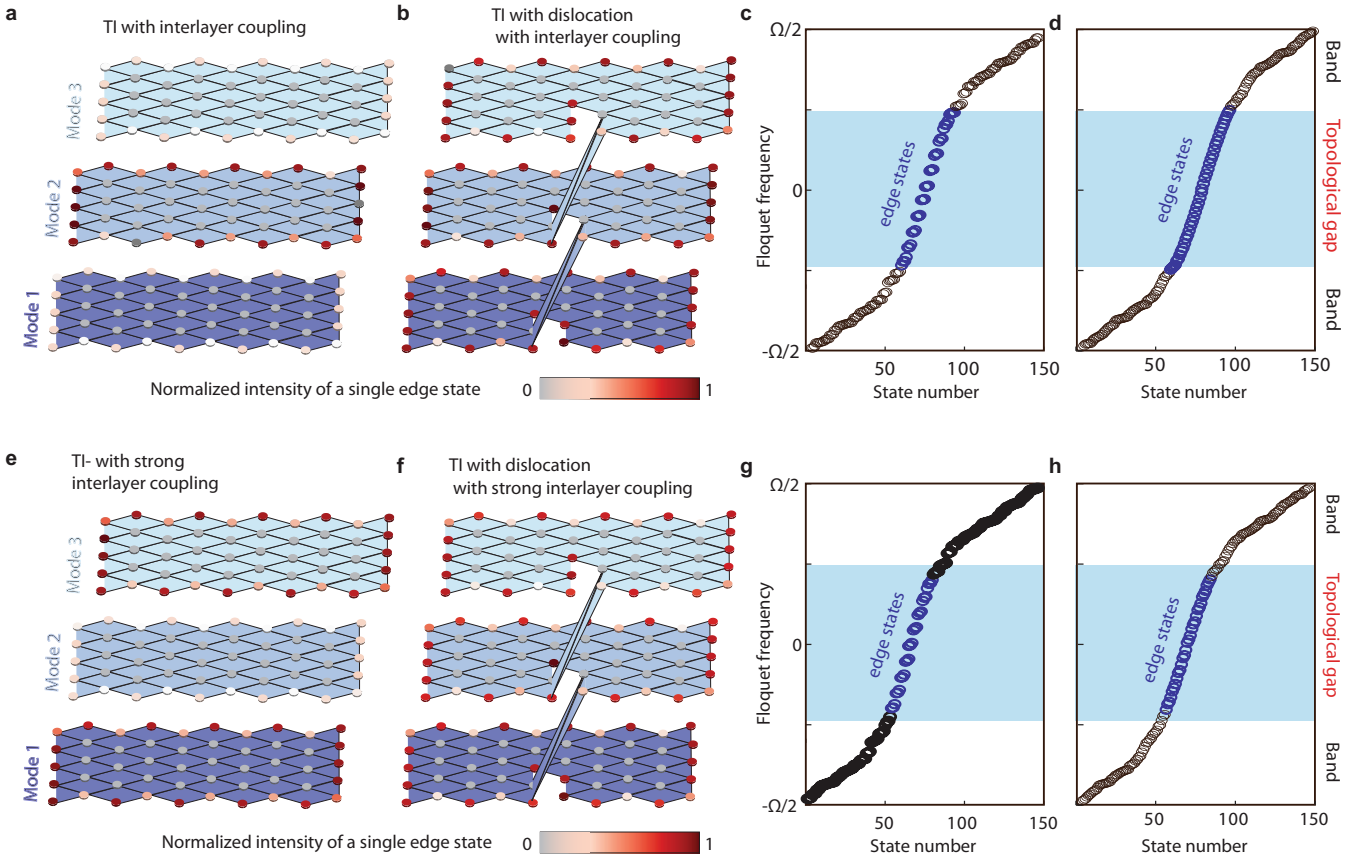

Extended Data Fig. 2 | Spectrum of the topological surface states and their typical structure in the presence of intermodal coupling. a, The amplitude as a function of location and mode in the 3D synthetic space without dislocation for moderate intermodal coupling of 20% of the spatial coupling. **b**, Same as **a** but for a lattice with a dislocation. **c**,**d**, Floquet spectrum as a function of the state number of **a** and **b**, respectively. **e**–**h**, Same as **a**–**d** but for strong intermodal coupling of 60% of the spatial coupling.